2-7-2006

Dynamic Contact Angle in Rim Instability of Dewetting Holes

Sung-Hwan Choi

Bi-min Zhang Newby
University of Akron Main Campus, bimin@uakron.edu

Dynamic contact angle in rim instability of dewetting holes

Sung-Hwan Choi and Bi-min Zhang Newby[a)]
Department of Chemical Engineering, The University of Akron, Akron, Ohio 44325-3906

(Received 23 September 2005; accepted 5 December 2005; published online 1 February 2006)

The effects of dynamic contact angle (θ_d), between a substrate and the melt of a dewetting polymer thin film, on the evolution of rim instabilities of dewetting holes were reported. Various θ_d's were achieved by covering SiO_x surfaces with different coverage of octadecyltrichlorosilane. On each surface, the morphology of the dewetting holes was examined in detail as the hole grew to a certain size. Rim instabilities, in terms of undulations in both r and z directions, became more pronounced as θ_d increased, under which condition, narrower and higher rims were also observed. Experimentally, atomic force microscopic scans of the rim were used to obtain the rim profile, which was predicted using θ_d. The predicted rim profile was used, in combination with the analysis of Rayleigh instability of a cylindrical fluid, to interpret the rim instability. The model captures the basic trend of the rim instability dependency on θ_d. The study demonstrates the importance of the substrate properties on the rim instability and the destabilization of polymer thin films during hole growth. © *2006 American Institute of Physics*. [DOI: 10.1063/1.2162534]

I. INTRODUCTION

Instability of polymer thin films ($<\sim 100$ nm) has strongly impacted the applications of these thin films. The failure of thermal stability and continuity, termed "dewetting," of polymer thin films has led to extensive studies of the dewetting phenomena.[1–4] Recently, construction of three-dimensional micro-nanoscaled polymer structures utilizing dewetting phenomena has also been demonstrated. Dewetting of polymer thin films in a controlled manner, with patterned substrates[5–7] or physical confinements,[8,9] facilitates the production of such structures, which then provide avenues for fundamental studies and practical applications. In order to achieve the desired structures using a dewetting process, a comprehensive understanding of the key factors affecting the dewetting process is essential. One such factor is the substrate surface properties, such as the surface energy. Studies[10–14] have shown that substrate surface properties affect the early stages of dewetting, such as the nucleation and growth of dewetting holes. In this paper, we focus on how the surface conditions, especially the substrate surface energy, control the formation and development of rims around the dewetting holes during their lateral growth.

During lateral growth of dewetting holes, the polymeric materials removed from the dewetting holes accumulate mostly along the circumference of the exposed substrates, forming ringlike polymer ridges called "rims."[1] In most dewetting studies, the rims are found to grow evenly in size with the growth of dewetting holes, without altering the overall profile.[14–16] However, for cases when large equilibrium contact angles occurred[1,12,15] or high molecular weight polymers were used,[1,17,18] it was observed that this retracting rim became unstable with fluctuations in the rim geometry. In some cases, the fluctuations in rim profile even caused the formation of "fingers," which were extended behind the rim growth. This rim instability is believed to be analogous to the Rayleigh instability, which accentuates the destabilization of cylindrical liquids into isolated droplets.[19,20]

Similar instabilities have been observed in the spreading of thin polymer or liquid films.[21–24] Both theoretical modeling and simulations have elucidated instabilities in terms of their driving forces. The driving force for a dewetting process is the spreading coefficient,[10] which is directly related to the surface energies of the substrate and the dewetting liquid, and subsequently the contact angle (θ) of the dewetting liquid forms on the substrate. However, few experimental studies, regarding the effects of this driving force[13] on the rim instability during the dewetting process, have been systematically performed. To our best knowledge, the only documented substrate effects on polymer thin-film dewetting behaviors involved the use of a fully nonpolar organosilane-covered substrate and two different types of silicon wafer.[1,17] Therefore, in this study, the evolution of the rim instability as a function of the dynamic contact angle (θ_d) of the dewetted polymer melt formed on the substrate will be followed, and an analysis of the rim instability based on Rayleigh instability will be presented.[25]

II. EXPERIMENTAL SECTION

Substrates with different surface energies were generated by contact printing (CP) of a methyl-terminated organosilane, *n*-octadecyltrichlorosilane (OTS, from Gelest Inc.), onto cleaned SiO_x surfaces to achieve different OTS coverage. Planar silicone stamps used for CP were fabricated using Sylgard® 184 purchased from Dow Corning. The standard procedures can be found elsewhere.[10] The masters used for fabricating the stamps were pieces (1×1 cm^2) of fluorosilane-modified silicon wafers. The "ink" for CP was a 2 mM solution of OTS in HPLC-graded hexane (J.T. Baker). The substrates, silicon wafers [P(100), Silicon Quest Interna-

a)Author to whom correspondence should be addressed. Electronic mail: bimin@uakron.edu

tional], were cleaned using the freshly prepared piranha solution and then oxidized using a UV/ozone treatment (UV/O cleaner model 42, Jelight) for 6 min. A planar stamp "inked" with the OTS solution was brought into contact with each substrate for contact times between 1 and 120 s. Polystyrene (PS; molecular weight, M_n=9.3k, PI=1.13, from Polymer Source, Inc.) thin films with a film thickness (δ) of ~800 Å were placed onto the OTS-modified surfaces using the "float-off and pickup" method.[17] The samples, after drying under ambient conditions for 15 h and then in a vacuum oven at 80 °C for 15 h, were annealed at 160 °C in air, while the hole growth was monitored using an optical microscope (Infini Tube, Edmond Scientifics). Annealing was terminated when the hole diameter reached certain chosen sizes (e.g., ~35 or 55 μm), and then the samples were quenched to room temperature to preserve hole morphology. A separate experiment (by gel permeation chromatography analysis) showed that thermal degradation of the PS thin films after annealing at 160 °C in air was insignificant within the annealing time of interest (<10 min). The overall morphology of the dewetting holes was characterized using optical microscopy (IX-70, Olympus) with a differential interference contrast (DIC) prism and an analyzer to enhance color [black and white with a monochrome charge-coupled device (CCD) camera] contrast in the rim height fluctuation. The rim height (h), the rim width (w), and the dynamic contact angle (θ_d) between the substrate and the PS melt at a dewetting hole diameter (D) of ~35 μm were obtained by atomic force microscopy (AFM, MI 2000 from Molecular Imaging) in noncontact mode. The instability wavelength (λ), or the spacing between the protrusions, was obtained by dividing the angular length of rim (circumference at the middle of rim width) at D of ~55 μm by the number of protrusions formed along the rim. Optical microscopic images of at least 50 well-defined dewetting holes (D~55 μm) formed on the substrates (two or three replicates) with a specific OTS coverage were taken and analyzed to obtain the angular length of the rims and the number of protrusions. The number of discernible protrusions or "nodes,"[26] which were easily noticed along the rim by clear color contrast and/or their multiple color bands, was manually counted from optical microscopic images. λ was estimated by dividing the circumference of the rim by the number of protrusions along the rim.

III. RESULTS AND DISCUSSION

Rims of dewetting holes of PS thin films on substrates having various OTS coverage, achieved by contact printing of OTS with different contact times, were examined. PS (M_n=9.3k) having a molecular weight much less than the entanglement weight of PS (M_e~19k), was chosen to minimize the slippage at the PS/substrate interface,[13,27] which, if present, might induce a great deal of complexity in rim instability.[28] The morphology and rim profile of the dewetting hole, specifically, h, w, and θ_d of the rim on the substrates (Fig. 1), were evaluated. The spacing between height fluctuations along the rim (λ) was also characterized. All these quantities were compared with the analysis based on Rayleigh instability, and qualitative agreements were found.

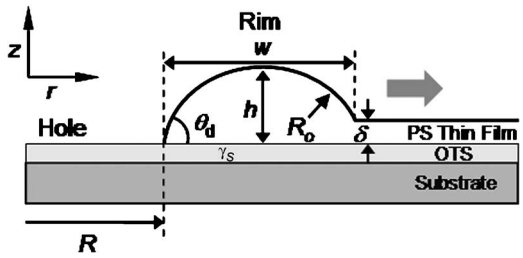

FIG. 1. Schematic of the cross-sectional profile of a dewetting hole. θ_d represents the dynamic contact angle formed by the polymer melt on the substrate. h, w, and R_o are the respective height, width, and radius of curvature of the rim, R is the radius of the dewetting hole. The sketch is not scaled, i.e., $h \ll w$.

A. Substrate-dependent rim morphology

The substrate-dependent rim instability of dewetting holes is presented in Fig. 2. A few distinguished hole morphological features were observed. For short contact times (<10 s) (low OTS coverage or high substrate surface energies, thus low θ_d's), relatively circular dewetting holes [Fig. 2(a)] with slight irregularity on the inside edge were observed. The darker colored ring around the outside edge of the rim indicated a slight decrease in height from the original film thickness.[15] The rim appeared to be relatively wide with some color bands (black-light gray-dark gray), indicating small undulation in its height. For a substrate contact printed with OTS for ~20 s [Fig. 2(b)], in addition to a reduction in w as compared to Fig. 2(a), more color bands (black-light gray-dark gray-light gray) with a smaller gap between the bands were also observed, indicating an increase in h. As the

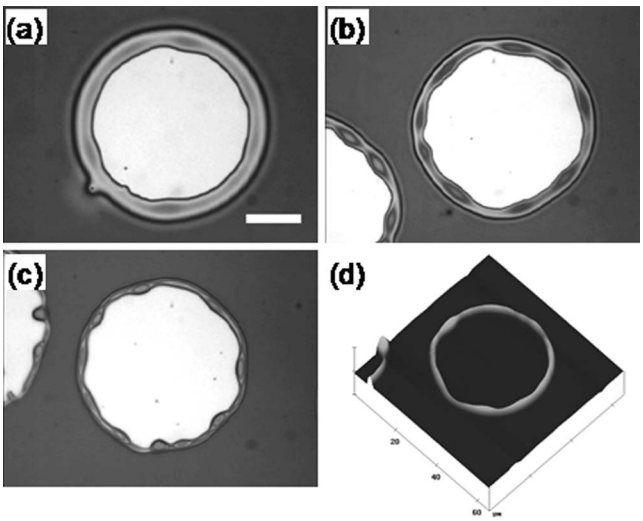

FIG. 2. Optical microscopic [(a)–(c)] and AFM (d) images of dewetting holes of PS-9.3k thin films formed on various substrates—each has a particular OTS coverage. The substrates were (a) 1 s contact printed OTS surface, (b) ~20 s contact printed OTS surface, and (c) and (d) ~120 s contact printed OTS surface. As contact time increased (more OTS molecules deposited to the surface, and a lower surface energy was resulted), the instability along the rim became more pronounced. The slight distortion in the bottom left corner of the rim seen in (a) is the result of a dust particle presented in the film. The dewetting holes imaged by the optical microscope have a similar diameter of ~55 μm. The scan size for (d) was 60 $\times$60 μm^2, the z scale was 1 μm/div. For the AFM scan, a hole with a diameter of ~35 μm was chosen to ensure the rim instability has not been fully developed, so the clear rim geometry can be obtained.

contact time increased, w continued to decrease while h continued to increase. Furthermore, along the rim, protrusions (portions with more color bands) in the height or the z direction and circumferential undulations in the r direction occurred. Protrusions in the z direction further developed and became pronounced enough for the inner part of the rim to bulge slightly in the opposite direction of the rim growth as the contact time increased to ~120 s [Fig. 2(c)]. A transition of the protrusion shape from long mounds along the angular direction [Fig. 2(b)] to compact "humps" [Fig. 2(c)] was also observed. The humps were more developed on substrates with higher coverage of OTS (i.e., longer contact times, greater θ_d's), and these evolved protrusions were eventually left behind from the rim as the rim developed and became "fingers."[1] For holes with a similar size, the amount of polymer melt removed from the hole, i.e., accumulated into the rim, should be similar; therefore, the above observations indicate that the substrate properties (e.g., surface energy) appeared to determine the allocation of the accumulated melt within the rim.[29]

The formation of protrusions, in a sense, was similar to the propagation of Rayleigh instabilities.[1,3,18] The rim would tend to break and form isolated droplets to minimize its system energy; however, it was constrained by the undewetted film outside the rim. As a result, the protrusions formed due to the instability had to grow in the z direction as well as inward in the r direction. For a substrate covered with even more OTS molecules (contact printed time >120 s), short fingers emerged from the unstable rims (not shown), and the rim instability was so pronounced that the circumference of the rim became irregular or "flower shaped."[1]

B. Predicting rim profile based on dynamic contact angle

In order to correlate the rim instability of dewetting holes to the Rayleigh instability, the rim profile needs to be determined. The rim profile in the rz plane likely depends on the dynamic contact angle of the polymer melt formed on the substrate, θ_d. θ_d controls the slope of the rim formed on the substrate, and thus may govern the profile of the rim. The experimental values of θ_d were obtained from the cross-sectional profiles of the AFM scans of dewetting holes. Holes with a particular size (~35 μm) on substrates having different OTS coverage were scanned [Fig. 2(d)]. This hole size was chosen to ensure that mature rims[30] had been developed while minimizing fluctuations that could alter the true value of θ_d. h and w, as defined in Fig. 1, were also obtained experimentally from the AFM images, and plotted against the experimental θ_d, and as θ_d increased, h increased, while w decreased (Fig. 3).

The rim profile (w and h on a particular OTS surface) can also be predicted using a material balance and the value of θ_d. The volume of PS removed from a dewetting hole should be accumulated into the rim (Fig. 1), and the volume of the hole and that of the rim are, respectively,

$$\pi\delta\left(R^2+\frac{\delta R}{\tan\theta_d}+\frac{1}{3}\frac{\delta^2}{\tan^2\theta_d}\right), \tag{1}$$

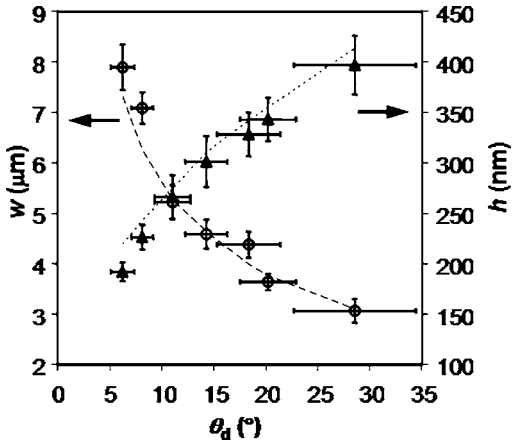

FIG. 3. Experimentally measured rim width (w, denoted as ○) and rim height (h, denoted as ▲) are plotted against θ_d. Dewetting holes with a similar size (D~35 μm) were chosen to minimize any size effect on the development of instability. As θ_d increased, w deceased while h increased. The anticipated h and w corresponding to each θ_d were estimated using a material balance [Eqs. (1)–(3)] with the measured θ_d and D values. The experimentally measured w and h agreed reasonably well with the anticipated h (dotted line) and w (dashed line) values. The error for each measured value was the standard derivation of at least ~50 measurements.

$$2\pi\left(R+\frac{1}{2}\left(w+\frac{\delta}{\tan\theta_d}\right)\right)SA, \tag{2}$$

where δ(~80 nm) is the thickness of the initial film, R is the radius of the dewetting hole, and SA is the cross-sectional area of the rim, which has the following form:

$$\frac{1}{4}\left(w+\frac{\delta}{\tan\theta_d}\right)^2\left(\frac{1}{\sin^2\theta_d}\right)\left(\theta_d-\frac{1}{2}\sin 2\theta_d\right)-\delta w. \tag{3}$$

The material balance Eqs. (1)–(3) along with the experimentally measured R and θ_d were used to estimate the anticipated w. The expected w for each θ_d (dashed line in Fig. 3) matches well with the measured value. The anticipated h can also be estimated from the anticipated w with a relationship [Eq. (4)] derived from the rim geometry,

$$h=\frac{1}{2}\left(w+\frac{\delta}{\tan\theta_d}\right)\left(\frac{1}{\sin\theta_d}-\frac{1}{\tan\theta_d}\right), \tag{4}$$

and the values (dotted line in Fig. 3) also agree reasonably well with the measured values.

C. Rim instability and Rayleigh instability

The rim geometry can be predicted using Eqs. (1)–(4) for holes with known sizes (D). Rims with higher aspect ratios (h/w) seem to be more susceptible to thermal fluctuations and become unstable at an earlier stage of hole growth. This agrees with the quantitative analysis on the growth of the rim instabilities using Rayleigh instability.

In most Rayleigh instability cases, a cylindrical liquid column is surrounded by a medium, and fluctuations are developed along the surface of the liquid, eventually leading the liquid column to break up and form droplets. It can be imagined that the rim around dewetting holes is a liquid thread in the form of a ring. Sekimoto *et al.*[31] pointed out that this ridge geometry is thermodynamically unstable

against surface fluctuations and exhibited behavior like the Rayleigh instability. However, some distinct features in the case of rim instability exist and need to be noted. First, the rim of a dewetting hole is not stationary as in the Rayleigh instability; the rim continuously expands in both w and h as the dewetting hole grows. Second, one side of the rim is attached to an undewetted film making it harder to break the rim into droplets under fluctuations. Third, the rim is not a cylindrical column; instead it is a flat cylindrical cap with a very small height and a large width. Fourth, the rim is exposed to two media instead of one for Rayleigh's case. While its curved surface is exposed to air, its base is in contact with a solid substrate.

For Rayleigh instability of a cylindrical liquid thread surrounded by another liquid medium, the growth rate (q) of the distortion or instability[19,25,31] is defined as

$$q = \frac{\gamma_{\mathrm{lm}}\Omega(\lambda,p)}{2R_o\mu_m}, \tag{5}$$

where γ_{lm} is the interfacial tension between the liquid and the medium, $\Omega(\lambda,p)$ is a complex function of the instability wavelength (λ) and the ratio (p) of the viscosity of the liquid column (μ_l) and the surrounding medium (μ_m), and $2R_o$ is the diameter of the liquid column. In our case, where the rim sits on the substrate with the curved portion exposed to air (Fig. 1), the growth rate will be quite different for the air side versus the substrate side. On the substrate side, the viscosity of the substrate (silicon wafer) is assumed to be approaching infinity while all other terms in Eq. (5) have a finite value. As a result, the growth of the protrusion is almost completely suppressed, and only q of the air side is important in the development of the instability. In the case of a large p ($p \rightarrow \infty$), q depends primarily on the liquid properties, and according to Tomotika, the expression becomes[19]

$$q = \frac{\gamma_{\mathrm{lm}}\Gamma(\lambda,R_o)}{2R_o\mu_l}. \tag{6}$$

When the surrounding medium is air, the value of $\Gamma(\lambda,R_o)$ is 1/3 and Eq. (6) can be simplified to Rayleigh's original expression for the instability of a cylindrical column of fluid in air,[20]

$$q = \frac{\gamma_{\mathrm{lm}}}{6R_o\mu_l}. \tag{7}$$

In our case, R_o is the radius of curvature of the rim as indicated in Fig. 1. Our rim consists of PS melt at 160 °C, or $\gamma_{\mathrm{lm}}=\gamma_{\mathrm{PS}}\cong 30.6$ mJ/m^2,[32] and $\mu_l=\mu_{\mathrm{PS}}\cong 103.8$ Pa s.[33] One might expect that the shear thinning behavior of the polymer could affect the viscosity for the cases when the dewetting velocity (dR/dt) is large ($\sim$235 μm/min). According to our calculation, the dimensionless strain rate parameter[34] is much smaller than 10, indicating the effects of dewetting velocity are unimportant to the viscosity of the polymer melt, and the zero shear viscosity can be used for all the calculations.

By using the predicted w and h at each θ_d, R_o and subsequently q values can be estimated from Eq. (7) and plotted as a function of θ_d in Fig. 4. In general, for a particular D, the instability grows faster as θ_d increases; consequently,

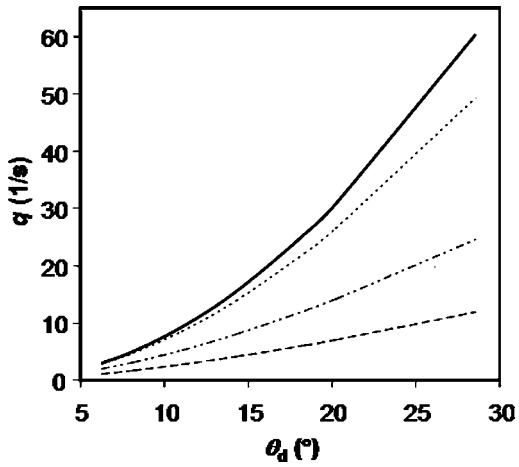

FIG. 4. Growth rate (q) of the rim instability is plotted as a function of θ_d. The value of q was calculated from Eq. (7). The curves from the top to the bottom correspond to D of 0.1, 1, 10, and 55 μm, respectively. For a fixed D, as θ_d increases, q increases.

more pronounced protrusions are expected. As shown in Fig. 4, q is substantially larger at a higher θ_d, especially when the hole size is smaller. For PS thin films used in our study ($\delta \sim 80$ nm), the dewetting is likely initiated with fluctuations of the film. The fluctuations grow toward the substrate and finally reach the substrate to form the dewetting holes, and then the holes grow laterally. As soon as the bottom of the fluctuation hits the substrate, a certain rim width, defined as the initial rim width, reaches. The value of the initial rim width depends on θ_d. As θ_d increases, the initial rim width decreases. For instance, the initial rim width is $\sim$2.89 μm for $\theta_d \sim 6°$, while it is 0.67 μm for $\theta_d \sim 29°$. The relative increases of w and h are smaller for a smaller θ_d. This is why the q value converges for θ_d less than 10°. For the cases with larger θ_d's ($>10°$), as the dewetting hole grows larger, a decrease in q occurs, since the relative increases of w and h are greater for these cases. Once the hole grows larger than 10 μm, the relative increase rates of w and h become comparable for different systems, and the q vs θ_d curve becomes less steep.

For a larger θ_d, q is always greater as compared to that of a smaller θ_d; hence, the rim instability becomes observable earlier or with a smaller dewetting hole, and more pronounced rim instability is expected for similar sized dewetting holes. To further verify this statement, one could estimate the time required for a certain amplitude of protrusion (i.e., $\sim$25 nm)[35] to be microscopically observable by adopting the expression for estimating the breakup time [t_b, $t_b = 1/q \ln(\alpha_b/\alpha_0)$, where α_b is the amplitude at breakup and α_0 is the original amplitude] of a stationary liquid cylinder.[25] Substituting the q value predicted using R_o when the fluctuation reaches the substrate, 25 nm for α_b and 0.3 nm for α_0,[25] the instability should become observable in $\sim$1.5 s for $\theta_d \sim 6°$ and $\sim$0.1 s for $\theta_d \sim 29°$. Experimentally, for $\theta_d < 11°$, the rim instability became microscopically observable[35] only after the dewetting hole grew greater than $\sim$10 μm, which took tens to hundreds of seconds after the initial hole was formed. Even with the highest θ_d (29°), the

emergence of the observable rim instability was still one order of magnitude lower than the analysis predicted.

As mentioned earlier, the analysis was oversimplified; many factors in our polymeric systems could slow down the development of the rim instability, which were not considered in the analysis. The continuous addition of material flow into the rim could dampen out some of the destabilizing process caused by capillary fluctuations. The rim, resembling a very small portion of the cylindrical geometry, is strictly confined by the substrate and connected to the continuous undewetted polymer film that retards the development of the rim and its instability. Therefore, the rim instability proceeds much slower than the Rayleigh model predicted. Nevertheless, the basic trend of the θ_d (or substrate surface energy) effect on the development of the rim instability was well captured, qualitatively, with the analysis based on Rayleigh instability.

Another worth noting quantity for the instability is the "instability wavelength," λ,[36] which was also determined using optical microscopic images as those shown in Fig. 2. The ratio of $\lambda/2R_o$ can be used to evaluate the validity of the theoretical predications. For the systems examined in this study, $\lambda/2R_o$ was found to vary from 0.4 to 2.2, which was much smaller than the value (4.51) reported for Rayleigh's instability cases.[20] Interestingly, when λ was divided by estimated w,[23] the ratio was between 3.6 and 4.6, which, for most of them, was slightly smaller but comparable to the value of the Rayleigh instability of a cylindrical thread in air.[20] The exact reason behind the agreement is unclear. Nonetheless, the authors do not feel it is adequate to replace $2R_o$ with w in Eq. (7), otherwise the effect of h or θ_d on rim instability would be neglected. For all the dewetting holes studied, the maximum aspect ratio (h/w) is 0.13 (Fig. 2), suggesting the height contribution to rim instability could be small, but not negligible. For example, with a similar w ($\sim$4.06 μm), h for $\theta_d \sim 29°$ ($\sim$0.50 μm) is almost four times of that for $\theta_d \sim 6°$ ($\sim$0.13 μm), and the corresponding values of D were $\sim$58 μm for $\theta_d \sim 29°$ and $\sim$6 μm for $\theta_d \sim 6°$. With these dimensions, much greater rim instability was observed for the dewetting holes formed with a higher θ_d.

IV. CONCLUSIONS

Rim instabilities of dewetting holes, developed during the dewetting of PS-9.3*k* thin films from various substrates that the polymer melt formed dynamic contact angles (θ_d) ranging from $\sim$6° to $\sim$29°, were investigated. As θ_d increased, more distinct instability was observed with enhanced protrusions in both the height and the radial directions. A transition from clean circular holes with even rims to holes with rims that have slight circumferential undulations and height fluctuations was observed at θ_d around 8°. The evolution of protrusions into pronounced features with small "fingers" occurred at $\theta_d \geqslant 29°$.

A simplified analysis based on the Rayleigh instability of viscous cylindrical fluids was applied to explain the rim instability dependency on θ_d. The analysis also utilized the rim profile predicted based on θ_d, which determined the slope of the inner rim. This simple model was capable of capturing the basic trend of θ_d-dependent rim instability. However, the experimentally observed rim instability development was about one order of magnitude slower than the model predicted. The discrepancies between the experimental data and the theoretical prediction likely resulted from some of the detailed geometric and polymeric properties that were not included in the model. A more comprehensive study can be conducted by including some of these details, which may provide a better guide to understand the development of rim instabilities and other instabilities occurring during the dewetting of polymer thin films. Nevertheless, this study pointed out that, in addition to the properties of polymer thin films, substrate surface properties, e.g., surface energy and subsequently the contact angle between the polymer melt and the substrate, which have received little attention in the past, should be included in theoretical analyses of polymer thin film behavior.

ACKNOWLEDGMENTS

We are grateful for the financial support from the Start-Up Fund from the College of Engineering and the Department of Chemical Engineering at The University of Akron. We also would like to thank Dr. Seung-ho Moon at National Institute of Standards and Technology for valuable discussion on the SPM imaging, and Dr. Shi-Qing Wang at the University of Akron for his insights on the interfacial slippage of polymer melts.

[1] A. Sharma and G. Reiter, J. Colloid Interface Sci. **178**, 383 (1996).
[2] P. F. Green and V. Ganesan, Eur. Phys. J. E **12**, 449 (2003).
[3] U. Thiele, Eur. Phys. J. E **12**, 409 (2003).
[4] P. Muller-Bauschbaum, J. Phys.: Condens. Matter **15**, R1549 (2003).
[5] Z. Zhang, Z. Wang, R. Xing, and Y. Han, Surf. Sci. **539**, 129 (2003).
[6] Y. Xia, D. Qin, and Y. Yin, Curr. Opin. Colloid Interface Sci. **6**, 54 (2001).
[7] E. Meyer and H. G. Braun, Macromol. Mater. Eng. **276/277**, 44 (2000).
[8] K. Y. Suh, J. Park, and H. H. Lee, J. Chem. Phys. **116**, 7714 (2002).
[9] S. Harkema, E. Schaffer, M. D. Morariu, and U. Steiner, Langmuir **19**, 9714 (2003).
[10] S.-H. Choi and B. Zhang Newby, Langmuir **19**, 1419 (2003).
[11] K. R. Shull and T. E. Karis, Langmuir **10**, 334 (1994).
[12] I. Karapanagiotis, D. F. Evans, and W. W. Gerberich, Colloids Surf., A **207**, 59 (2002).
[13] F. Brochard-Wyart, P.-G. de Gennes, H. Hervert, and C. Redon, Langmuir **10**, 1566 (1994).
[14] G. Reiter, Phys. Rev. Lett. **68**, 75 (1992).
[15] R. Seemann, S. Herminghaus, and K. Jacobs, Phys. Rev. Lett. **87**, 196101 (2001).
[16] G. Reiter, Phys. Rev. Lett. **87**, 186101 (2001).
[17] G. Reiter, Langmuir **9**, 1344 (1993).
[18] J.-L. Masson, O. Olufokunbi, and P. F. Green, Macromolecules **35**, 6992 (2002).
[19] S. Tomotika, Proc. R. Soc. London, Ser. A **150**, 322 (1935).
[20] L. Rayleigh, Philos. Mag. **34**, 145 (1892).
[21] S. M. Troian, E. Herbolzheimer, S. A. Safran, and J. F. Joanny, Europhys. Lett. **10**, 25 (1989).
[22] F. Melo, J. F. Joanny, and S. Fauve, Phys. Rev. Lett. **63**, 1958 (1989).
[23] R. Vuilleumier, V. Ego, L. Neltner, and A. M. Cazabat, Langmuir **11**, 4117 (1995).
[24] A. M. Cazabat, F. Heslot, S. M. Troian, and P. Carles, Nature (London) **346**, 824 (1990).
[25] P. H. M. Elemans, J. M. H. Janssen, and H. E. H. Meijer, J. Rheol. **38**, 1311 (1990).
[26] Y. Asano, A. Hoshino, H. Miyaji, Y. Miyamoto, and K. Fukao, "Pattern

formation by rim instability in dewetting polymer thin films," in *Nonlinear Dynamics in Polymeric Systems*, ACS Symposium Series 869, edited by A. J. Pojman and Q. Tran-Cong-Miyata (American Chemical Society, Washington, DC, 2004), p. 186.
[27] C. Redon, J. B. Brzoska, and F. Brochard-Wyart, Macromolecules **27**, 468 (1994).
[28] A. Muench, J. Phys.: Condens. Matter **17**, S309 (2005).
[29] A separate experiment was performed to rule out the dewetting velocity (V_h) effect on the rim instability. Thin films on the substrate with contact printing of OTS for ~120 s were annealed at three different temperatures of 130, 150, and 160 °C to achieve various V_h. The rim instability of those holes grown under different V_h was similar, suggesting the rim instability was related to neither the hole growth rate nor the viscosity of the PS melt.
[30] F. Brochard-Wyart, G. Debregeas, R. Fondecave, and P. Martin, Macromolecules **30**, 1211 (1997).
[31] K. Sekimoto, R. Oguma, and K. Kawasaki, Ann. Phys. **176**, 359 (1987).
[32] S. Wu, J. Phys. Chem. **74**, 632 (1970).
[33] T. G. Fox and P. J. Flory, J. Polym. Sci. **14**, 315 (1954).
[34] W. W. Graessley, Adv. Polym. Sci. **16**, 1 (1974).
[35] The minimum height difference to be experimentally observed with the optical microscopy by color contrast was ~50 nm. The value was obtained from the height difference between protrusions and nonprotruding regions of the rim using the AFM scans.
[36] J. B. Fournier and A. M. Cazabat, Europhys. Lett. **20**, 517 (1992).